# A New OCT-based Method to Generate Virtual Maps of Vitreomacular Interface Pathologies

Agnieszka Stankiewicz[1],
Tomasz Marciniak[1], Adam Dąbrowski[1]

[1]Division of Signal Processing and Electronic Systems
Chair of Control and Systems Engineering
Faculty of Computing
Poznan University of Technology
Poznan, Poland,
e.g., tomasz.marciniak@put.poznan.pl

Marcin Stopa[2,3], Elżbieta Marciniak[2]

[2]Clinical Eye Unit, Heliodor Swiecicki University Hospital,
Poznan University of Medical Sciences
Poznan, Poland
[3]Department of Optometry and Biology of Visual System,
Poznan University of Medical Sciences
Poznan, Poland,
stopa@ump.edu.pl

*Abstract*— **Optical coherence tomography (OCT) is the most accurate modality for noninvasive assessment of vitreoretinal interface (VRI). The scientific objective of research presented in this paper was to develop a new OCT-based method for investigation of vitreomacular interface pathologies in human eyes. We propose a new approach for the automatic generation of virtual maps representing the distance between the posterior surface of the hyaloid (PSH) and the inner limiting membrane (ILM) in the vitreomacular traction (VMT) pathology. Volumetric data was acquired from 3 adult patients with VMT. OCT B-scans were processed frame-by-frame and refined by advanced digital imaging algorithms, including application of the graph analysis approach, that allow for plausible segmentation of epiretinal pathologies and retinal surface. We are able to precisely segment and quantify VMTs in all subjects. The resulting virtual maps show a potential to evolve into a new useful tool for eye doctors that can support clinical decisions.**

**Keywords - OCT, vitreoretinal interface, image processing, retinal layers segmentation**

## I. INTRODUCTION

Actually various non-invasive methods of eye observation are gaining significance in both medicine and biometry [1, 2, 3, 4]. Among them optical coherence tomography (OCT) has proved to be the most important non-invasive technique for tissue cross-section imaging using the light scattered on individual layers of the examined tissue [5]. Indeed, recently our understanding of various retinal disorders has been transformed with the OCT [6, 7, 8, 9]. Taking this into account, in this paper we propose a new OCT based approach to visualize vitreomacular interface pathologies.

Visual acuity deterioration, metamorphopsia and impairment of central vision are typical symptoms of a variety of diseases that affect the macula in humans. Several of them (vitreomacular traction, epiretinal membrane, lamellar macular hole, pseudohole, full-thickness macular hole) are associated with anomalous changes in vitreous, vitreoretinal interface and retinal architecture.

The vitreous body is the largest structure within the human eye. It is attached to the structures of the inner eye including the innermost layer of the retina i.e. internal limiting membrane (ILM). The vitreous body is contained within a cortex composed of dense collagen matrix. As the eye ages, vitreous gel liquefaction and weakening of vitreoretinal adhesion occur. These lead to progressive separation of the posterior vitreous cortex from the retina that is defined as posterior vitreous detachment (PVD).

In some cases, the abnormal adhesion of the vitreous cortex to the ILM is present (Fig. 1.) that can induce several serious pathologic events. Vitreomacular traction is one of them. Here posterior vitreous with adhesion to the macula exerts traction on the retina. Persistent traction can lead to deformation of the fovea, cystoid foveal thickening, and disorganization of retinal layers. An example of optical coherence tomography B-scan of VMT is illustrated in Fig. 2.

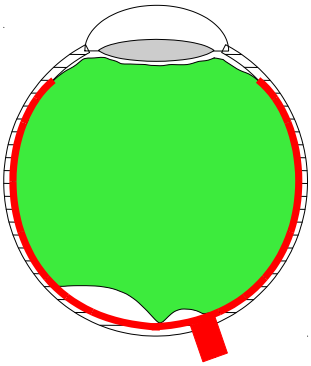

Figure 1. Initial stage of PVD: perifoveal vitreous detachment – the vitreous remains attached to the fovea, mid-peripheral retina, and optic disk; the abnormal adhesion of the vitreous cortex to the ILM in the fovea is present

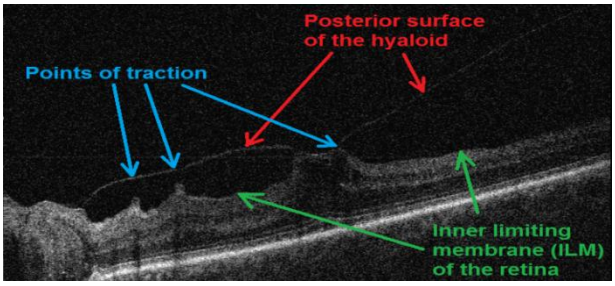


Figure 2. Example of OCT B-scan of a macula from a patient with VMT (image from the OCT database of Clinical Eye Unit, Heliodor Swiecicki University Hospital in Poznan)

Segmentation of retinal layers in OCT scans has been an important goal of image processing applications. Currently available reports have presented many algorithms, based on different approaches to address the issue of automated retinal segmentation. They can be divided into several groups. Among them the main are: peak intensity and gradient analysis [10, 11, 12], active contour modeling [13, 14], pattern recognition [15, 16], graph search techniques [17, 18, 19], kernel and clustering methods [20, 21, 22].

The automated segmentation of retinal layers is challenged by many aspects such as: multiplicative and neighborhood correlated noise, uneven tissue reflectivity caused by the low image contrast between adjacent retinal layers, vessels hypo-reflectivity, unexpected movement of the patient's eye that can be overcome by eye tracking solutions, device-dependence and the presence of pathology. In severe pathologies the algorithms fail in most cases due to heavily abnormal data samples. Development of a robust solution would be very beneficial, especially such that allows for the detection of various pathogenic changes in the retina and vitreoretinal interface. In the recent literature some approaches of computer aided analysis of the OCT images, aimed to automatically detect and assess pathological changes in the retina, can be found. However, these solutions are still rare and not sufficient for the purpose of the VRI analysis.

The proposed automated analysis requires a novel approach to precisely segment and quantify vitreoretinal interface pathologies. It will result in a new tool for eye doctors, that can support their clinical decisions.

## II. OCT-BASED GENERATION OF VIRTUAL MAPS

The proposed solution utilizes a 3D OCT cross-sections to generate a virtual profile map of one of vitreomacular interface pathologies i.e. the vitreomacular traction (VMT). All scans were acquired with the Copernicus HR device (OPTOPOL Technology, Sp. z o. o., Zawiercie, Poland) [23]).

The acquired series of 3D OCT volumetric data from the patients with VMT pathology were subjected to computerized automatic analysis using advanced digital imaging algorithms including application of the graph analysis approach [19].

The proposed algorithm (Fig. 3) consists of the following steps:

1. ILM line segmentation in every OCT B-scan
2. Segmentation of posterior surface of the hyaloid on a single OCT B-scan (further designated as the PSH line)
3. Calculation of distance between the segmented ILM line and the PSH line
4. Vessels structure segmentation from the reconstructed fundus image
5. Creation of a virtual map of the VMT profile.

These steps, presented in Fig. 3, are discussed below in detail.

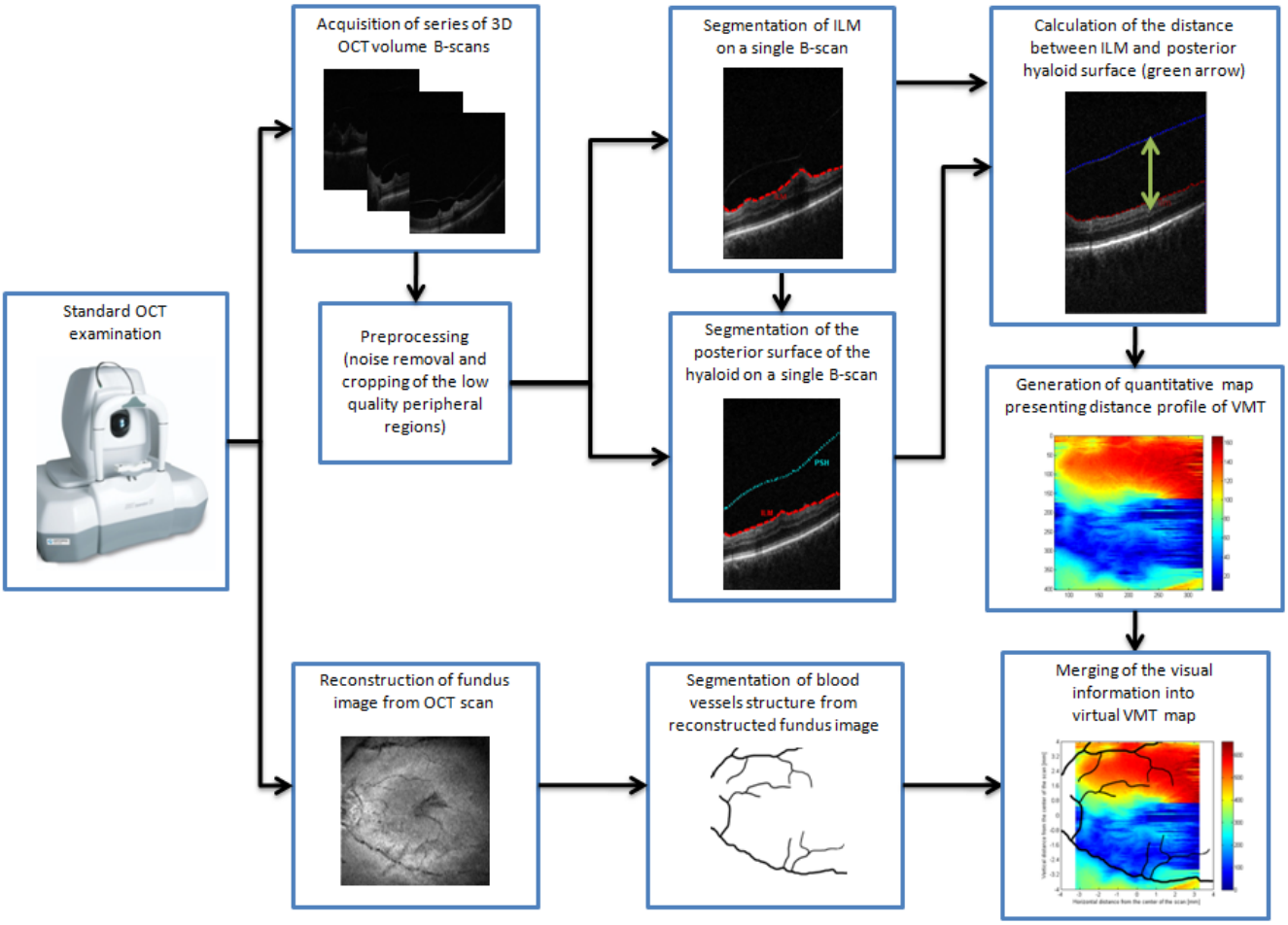


Figure 3. Overview of the proposed VMT segmentation algorithm

### A. *Internal limiting membrane( ILM) segmentation*

Segmentation of the ILM is based on the graph search theory implementation proposed in [19] and available at [24]. In this approach an OCT B-scan is represented as a graph of nodes, where each node corresponds to a B-scan pixel. A set of links connecting the nodes (called edges) form a path across the graph. To each edge a weight is assigned. These weights (values between 0 and 1), formed as a matrix, describe the distances between pixels and their intensity differences.

A necessary step for this algorithm requires selection of the start and end points for the segmented layer. The easiest way to fulfill this requirement is to automatically initialize these points at the upper-left and the bottom-right corners of the image.

The resulting segmentation of the ILM using this algorithm is illustrated in Fig. 4a.

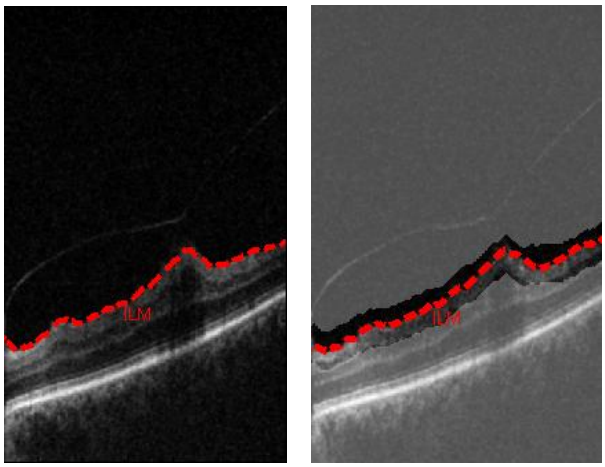


(a) (b)

Figure 4. Example of OCT B-scan of the macula from a patient with VMT (a) with the detected ILM marked as a red line and (b) with the narrow region of interest (ROI) visible as a dark lane along the found ILM line (image from the OCT database of Clinical Eye Unit, Heliodor Swiecicki University Hospital in Poznan)

#### 1) *Additional image cropping*

The described method is based on the assumption that the segmented layer extends across the entire width of the B-scan. Unfortunately, the acquired OCT images did not meet this requirement, thus additional cropping of the images was necessary. The experimentally selected regions to be discarded from the leftmost and rightmost image sides were set to 75 pixels at each side. This gives 18,75 % reduction of the total image width for our B-scans (of 800 pixels width resolution).

#### 2) *Determination of ROI from neighboring images*

The presented solution was sufficient for the most cases of the acquired OCT cross-sections. However, there were some occurrences of badly identified ILM boundaries. In such situations, due to heavily noisy signal, the produced ILM lines were located at the top of the image where obviously no retinal layer was placed.

We proposed a solution for elimination of such fatal errors, consisting in taking positions into account of the previously found ILM lines in the neighboring images. Thus, a reduced region of interest (ROI) for the search of ILM line in the next B-scan is introduced. This allows for removal of invalid boundaries prior to the graph cut. The maximum possible vertical distance between the ILM lines in subsequent B-scans was empirically determined as 20 pixels in each vertical side. The in this way defined ROI is indicated in Fig. 4b.

### B. *Posterior surface of the hyaloid (PSH) segmentation*

The segmentation of the posterior surface of the vitreous is done similarly to the previously described step and also uses the same graph search approach. However, for this structure a simplification of the search can be made due to the nature of the VMT pathology, i.e., that the posterior surface of the hyaloid is always above the already defined ILM surface on the OCT cross-section. Thus, a limitation of the graph weights to the valid search space can be made. An example of the correctly defined PSH line is illustrated in Fig. 5.

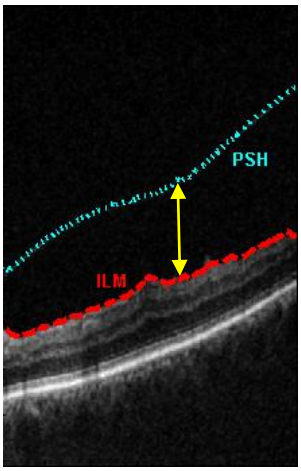


Figure 5. Example of correctly defined ILM and PSH surfaces on a single OCT B-scan (ILM and PSH lines) with annotation of the vertical distance between them (image from the OCT database of Clinical Eye Unit, Heliodor Swiecicki University Hospital in Poznan)

### C. *Calculation of distance vectors between ILM and PSH*

For each acquired OCT B-scan vertical distances (depths) between the vitreous and the surface of retina (i.e., between the ILM and PSH lines) are calculated (Figs. 3 and 5). This results in vectors of 650 depths for each OCT B-scan (original B-scans are 800 pixels wide, but they are cropped by 75 pixels from both the left and the right hand side, as already explained). The obtained $n$ distance vectors (for typically $n = 100$ B-scans) are further merged among all B-scans and analyzed for the purpose of finding the relevant adhesion areas (Section II.*E*).

### D. *Fundus vessels segmentation*

As mentioned earlier, the proposed imaging method takes into account both the thickness map and the fundus image based on the OCT B-scans. The most important elements of the fundus image are the properly segmented blood vessels. The vessel segmentation process was performed using the unsupervised learning method [25].

The Copernicus HR device gives a possibility to obtain the so-called reconstructed fundus image, which is an image created from a series of $n = 100$ B-scans. Vertical resolution of the directly reconstructed fundus image i.e., 800×100 pixels is quite low (as shown in Fig. 6a). Thus the finally reconstructed square 8 mm×8 mm fundus image has to be interpolated to the 800×800 resolution, e.g. with the use of the bicubic method (Fig. 6b).

Although a quality of such fundus image is still rather low, the main vessels can be successfully detected. Fig. 7 shows the results of such segmentation with the use of the multi-scale technique [26].

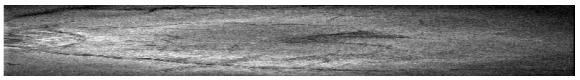

(a)

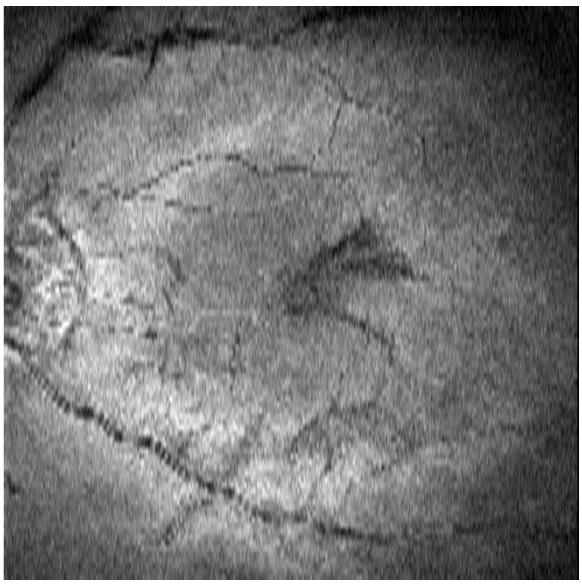

(b)

Figure 6. Example of reconstruction of fundus image from a series of OCT scans for a healty patient: (a) acquired image, (b) reconstructed fundus (image from the OCT database of Clinical Eye Unit, Heliodor Swiecicki University Hospital in Poznan)

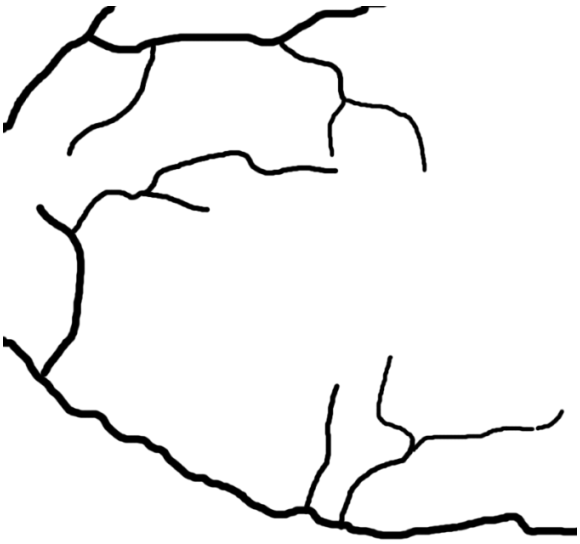

Figure 7. Example of vessels structure segmented from the reconstructed fundus image

### *E. Virtual map generation*

The distances derived in Section II.*C*, merged for all $n$ = 100 distance vectors are next visualized as a color depth map. The width, height, and depth of the resulting 3D data structure are described in [mm] for the width and height and in [μm] for the depth. This provides a clinician a very valuable information regarding the stage of posterior vitreous detachment in the examined region.

The final virtual map representing the distance profile for the VMT pathology in the region of macula is further illustrated in relation to the segmented structure of blood vessels from the reconstructed fundus image. Such virtual maps are presented in Figs. 8–10.

## III. EXPERIMENTS

The Copernicus HR device uses the spectral domain optical coherence tomography to obtain 3-dimensional cross-section images of the retina and vitreoretinal interface, and offers several scanning programs, 4–10 mm scan width and 2 mm scan depth.

During the experiment a volume of 100 OCT B-scans (cross-sections) was acquired from each patient. Each scan consisted of 800 A-scans, whereas each A-scan consisted of 1010 points. This resulted in a set of 100×800×1010 volume points representing the tissue structure of 8×8×2 mm in the central macula. Each OCT B-scan was then subjected to the analysis with the described algorithm.

Implementation of the described algorithm was carried out using the Matlab environment. The average computation time of the ILM and PSH lines segmentation were 0.44 s and 0.58 s per image, respectively. The experiment was conducted on a 64-bit PC workstation with Windows OS, Intel i7 processor at 2.70 GHz, and 4 GB RAM.

### *A. Database*

Patients were recruited by the team of participating physicians from the Clinical Eye Unit, Heliodor Swiecicki University Hospital in Poznan. The research was approved by the Bioethical Committee of Poznan University of Medical Sciences and all participants signed an informed consent document before enrollment. The study included a group of patients diagnosed with a VMT pathology. There were no inclusion/exclusion criteria based on sex and age. Each patient was subjected to the standard eye examination (assessment of best corrected visual acuity, anterior segment and dilated fundus slit-lamp examination) and standard OCT examination of the macula. All tests were non-invasive and were routine procedures for these types of diseases.

Volumetric data was acquired from 3 adults (one female and two males). Average age in the group was 69 years (ranging from 64 to 76).

### *B. Results*

The resulting virtual VMT profile maps for the tested subjects are shown in Figs. 8–10. They are composed of 100 vertical lines (each of 325 points) corresponding to the acquired B-scans. The colors of the image pixels represent the distances between the ILM and PSH lines at each point (in the so-called temperature scale). Scales on the right hand sides of these Figures show respective ranges for each color in [μm]. For example, the blue color suggests that the distance between ILM

and PSH layers is small (about 100 μm), while red color describes larger distance suggesting advanced detachment of the hyaloid.

As it can be observed, horizontal lines forming the VMT profile maps have artifacts and give an impression of some irregularity in the tissue structure. This is an illusion caused by somehow improper image segmentation. This phenomenon resulted from too low image quality and too noisy signal. In result, the graph-based algorithm could produce too smooth borders between each layer. This is incorrect in the case of the studied pathologies (as it can be noticed in Fig. 2).

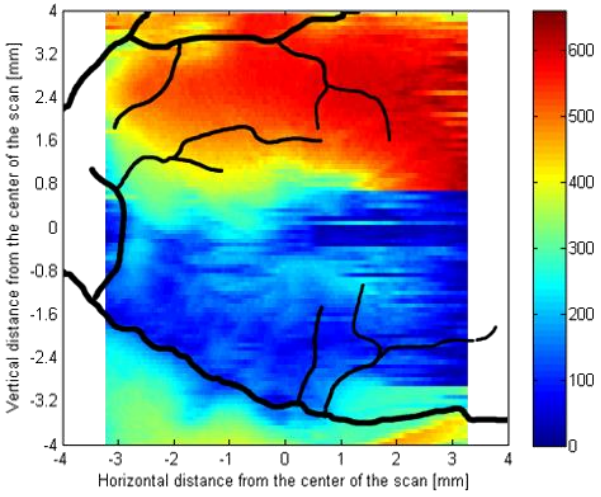


Figure 8. Virtual VMT profile map with respect to the vessels structure for patient GG (original image from the database of Clinical Eye Unit, Heliodor Swiecicki University Hospital in Poznan)

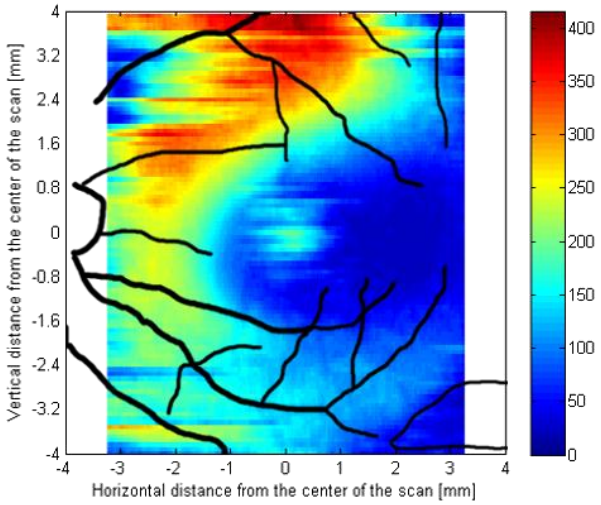


Figure 9. Virtual VMT profile map with respect to the vessels structure for patient HZ (original image from the database of Clinical Eye Unit, Heliodor Swiecicki University Hospital in Poznan)

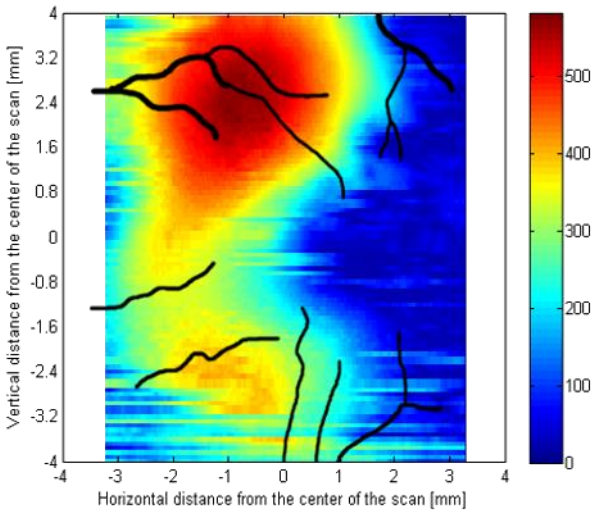


Figure 10. Virtual VMT profile map with respect to the vessels structure for the patient PZ (original image from the database of Clinical Eye Unit, Heliodor Swiecicki University Hospital in Poznan)

## IV. CONCLUSIONS

In this paper we have described a novel automated method of presenting profile of epiretinal abnormalities in relation to retinal surface (virtual maps of the fundus). This method relies on active contour modeling, pattern recognition, and graph search techniques. Our experiments suggest that the method is quite robust and can detect vitreoretinal interface pathologies properly (based on visual analysis of segmented B-scans). Nevertheless our observation is that resulting virtual maps showed some irregular vertical edges (Fig. 9.). This phenomenon is thought to be produced by some instability of the segmented layers among B-scans. This issue has to be addressed in our future studies. Current relatively low resolution of the final virtual maps can be improved by merging results of consecutive vertical and horizontal OCT examinations.

So far there are only spare studies on quantitative analysis of epiretinal pathologies. Kim et al. [27] aimed to quantify the displacement of macular capillaries using infrared fundus photographs and image processing software (ImageJ). Similar studies, which indirectly assumed retinal surface changes by measuring displacement of large retinal vessels, were carried out by other groups on conventional fundus photographs [28, 29]. Their studies have fundamental shortcomings, since their indirect approach results in low precision of quantification.

By now very few publications have investigated epiretinal abnormalities and retinal surface changes with quantitative analysis based on automated segmentation of the OCT cross-sections [30, 31].

The presented algorithm can be subjected to a series of OCT cross-sections acquired from any OCT device. It is important to notice that such a machine should also produce at least the reconstructed fundus image (necessary for reference of virtual map to the vessels structure).

We plan to improve the described solution by the application of advanced gradient analysis (for the detection of ragged parts of ILM layer caused by the traction occurrence)

and the correction of found ILM layer based on the tissue reflectivity of surrounding pixels.

The proposed virtual maps are meant to support diagnostic procedures to monitor progression of the disorder and to select case-appropriate treatment algorithms, giving eye doctors potentially new understanding of the investigated problems. Possibly they can serve as the basis for further studies on predictions of anatomical success with medical or surgical intervention. Furthermore they can provide guidance for safe positioning of surgical instruments in vitrectomy surgery not only for VMT but also others.

## REFERENCES


[1] Drexler W., Fujimoto J. G., Optical Coherence Tomography Technology and Applications, Springer-Verlag Berlin Heidelberg, 2008.

[2] Stopa M., Bower B.A., Davies E., Izatt J.A., Toth C.A., "Correlation of pathologic features in spectral domain optical coherence tomography with conventional retinal studies", Retina 28, pp. 298-308, 2008.

[3] Burge M. J., Bowyer K. W., Handbook of Iris Recognition, Springer-Verlag London, 2013.

[4] Marciniak T., Dąbrowski A., Chmielewska A., Krzykowska A., "Selection of parameters in iris recognition system", Multimedia Tools and Applications, Vol. 68, no 1, pp. 193-208, 2014.

[5] Huang D., Swanson E. A., Lin C.P., Schuman J. S., Stinson W. G., Chang W., Hee M.R., Flotte T., Gregory K., Puliafito C.A., Fujimoto J.G., "Optical coherence tomography", Science 254, pp. 1178-1181, 1991.

[6] Hee M.R., Izatt J.A., Swanson E.A., et al., "Optical coherence tomography of the human retina", Arch Ophthalmol. 113, pp. 325-332, 1995.

[7] Cense B., Nassif N., Chen T., et al., "Ultrahigh-resolution high-speed retinal imaging using spectral-domain optical coherence tomography", Opt Express 12, pp. 2435-2447, 2004.

[8] Srinivasan V.J., Wojtkowski M., Witkin A.J., Duker J.S., Ko T.H., Carvalho M., Schuman J.S., Kowalczyk A., Fujimoto J.G., "High-Definition and 3-dimensional Imaging of Macular Pathologies with High-speed Ultrahigh-Resolution Optical Coherence Tomography", Ophthalmology 113(11), pp. 2054-2065, 2006.

[9] Mumcuoglu T., Wollstein G., Wojtkowski M., Kagemann L., Ishikawa H., Gabriele M.L., Srinivasan V., Fujimoto J.G., Duker J.S., Schuman J.S., "Improved Visualization of Glaucomatous Retinal Damage Using High-speed Ultrahigh-Resolution Optical Coherence Tomography", Ophthalmology 115(5), pp. 782-789, 2008.

[10] Koozekanani D., Boyer K., Roberts C., "Retinal thickness measurements from optical coherence tomography using a Markov boundary model", Medical Imaging, IEEE Transactions on 20(9), pp. 900-916, 2001.

[11] Ishikawa H., Stein D.M., Wollstein G., Beaton S., Fujimoto J.G., Schuman J.S., "Macular segmentation with optical coherence tomography," Invest. Ophthalmol. Vis. Sci. 46(6), pp. 2012–2017, 2005.

[12] Fabritius T., Makita S., Miura M., Myllylä R., Yasuno Y., "Automated segmentation of the macula by optical coherence tomography", Opt. Express 17(18), pp. 15659–15669, 2009.

[13] Mishra A., Wong A., Bizheva K., Clausi D.A., "Intra-retinal layer segmentation in optical coherence tomography images", Optics Express 17(26), pp. 23719–23728, 2009.

[14] Tan O., Li G., Lu A.T.-H., Varma R., Huang D., A.I. for Glaucoma Study Group, "Mapping of Macular Substructures with Optical Coherence Tomography for Glaucoma Diagnosis", Ophthalmology 155(6), pp. 949-956, 2008.

[15] Kajic V., Povazay B., Hermann B., Hofer B., Marshall D., Rosin P. L., Drexler W., "Robust segmentation of intraretinal layers in the normal human fovea using a novel statistical model based on texture and shape analysis", Optics Express 18(14), pp. 14730–14744, 2010.

[16] Vermeer K., van der Schoot J., de Boer J., Lemij H., "Automated Retinal and NFL Segmentation in OCT Volume Scans by Pixel Classification", in ARVO 2010 Annual Meeting - Association for Research in Vision and Ophthalmology, Fort Lauderdale, 2010.

[17] Garvin M.K., Abramoff M.D., Kardon R., Russell S.R., Wu X., Sonka M., "Intraretinal Layer Segmentation of Macular Optical Coherence Tomography Images Using Optimal 3-D Graph Search", IEEE Transactions on Medical Imaging 27(10), pp. 1495–1505, 2008.

[18] Quellec G., Lee K., Dolejsi M., Garvin M.K., Abramoff M.D., Sonka M., "Three-Dimensional Analysis of Retinal Layer Texture: Identification of Fluid-Filled Regions in SD-OCT of the Macula", Medical Imaging, IEEE Transactions on 29(6), pp. 1321 –1330, 2010.

[19] Chiu S. J., Li X. T., Nicholas P., Toth C. A., Izatt J. A., and S. Farsiu, "Automatic segmentation of seven retinal layers in SDOCT images congruent with expert manual segmentation," Optics Express, vol. 18, no. 18, pp. 19413–19428, 2010.

[20] Fuller A. R., Zawadzki R. J., Choi S., Wiley D. F., Werner J. S., Hamann B., "Segmentation of Three-dimensional Retinal Image Data", IEEE Transactions on Visualization and Computer Graphics 13(6), pp. 1719–1726, 2007.

[21] Szkulmowski M., Wojtkowski M., Sikorski B., Bajraszewski T., Srinivasan V.J., Szkulmowska A., Kaluzny J.J., Fujimoto J. G., Kowalczyk A., "Analysis of posterior retinal layers in spectral optical coherence tomography images of the normal retina and retinal pathologies", Journal of Biomedical Optics 12(4), 2007.

[22] Cha Y. M., Han J.H., "High-Accuracy Retinal Layer Segmentation for Optical Coherence Tomography Using Tracking Kernels Based on Gaussian Mixture Model", IEEE Journal of Selected Topics in Quantum Electronics 20(2), 2014.

[23] SOCT Copernicus HR User Manual Software Version 4.3.0 User Manual rev. A 2011.

[24] Teng PY, Caserel, GitHub repository, 2014, http://pangyuteng.github.io/caserel.

[25] [Zhihong 2012] Zhihong Hu; Niemeijer, M.; Abramoff, M.D.; Garvin, M.K., "Multimodal Retinal Vessel Segmentation From Spectral-Domain Optical Coherence Tomography and Fundus Photography," Medical Imaging, IEEE Transactions on , vol.31, no.10, pp.1900-1911, , doi: 10.1109/TMI.2012.2206822, 2012.

[26] Vlachos, M.; Dermatas, E., "Multi-scale retinal vessel segmentation using line tracking," Computerized medical imaging and graphics : the official journal of the Computerized Medical Imaging Society 1 April 2010, volume 34, issue 3, pp. 213-227.

[27] Kim J.W., Choi K.S., "Quantitative analysis of macular contraction in idiopathic epiretinal membrane", BMC Ophthalmol, 2014 Apr 16, 14:51.

[28] Weinberger D., Stiebel-Kalish H., Priel E., Barash D., Axer-Siegel R., Yassur Y., "Digital red-free photography for the evaluation of retinal blood vessel displacement in epiretinal membrane", Ophthalmology, 1999 Jul, 106(7):1380-3.

[29] Yang H.K., Kim S.J., Jung Y.S., Kim K.G., Kim J.H., Yu H.G., "Improvement of horizontal macular contraction after surgical removal of epiretinal membranes", Eye (Lond). 2011 Jun;25(6):754-61.

[30] Lu W., Oakley J., Russakoff D., Chang R., "vitreo-retinal interface segmentation from spectral-domain oct using change detection and belief propagation", 2013 IEEE 10th International Symposium on Biomedical Imaging, San Francisco, pp. 1320-1323, 2013.

[31] Uji A., Murakami T., Unoki N., Ogino K., Nishijima K., Yoshitake S., Dodo Y., Yoshimura N., "Parallelism as a Novel Marker for Structural Integrity of Retinal Layers in Optical Coherence Tomographic Images in Eyes With Epiretinal Membrane", Am J Ophthalmol. 157(1), pp. 227-236, 2014.



The presented results were prepared mainly within the DS/2014 project.

This work was partly supported by the project ,,Scholarship support for PHD students specializing in majors strategic for Wielkopolska's development", Submeasure 8.2.2 Human Capital Operational Programme, co-financed by European Union under the European Social Fund.